Supplementary Material

1 LATTICE CONSTANTS

The equilibrium crystal lattice and atomic positions were found by minimizing the forces on the atoms and stresses in the crystal cell. The structural data shown here were obtained with the all electron code FHI-Aims Blum et al. (2009) and the PBEsol density functional, because of the good structural results. The reults were obtained with a tight setting and 10x10x10, 8x8x6, 6x6x6, and 3x6x6 grids of k-points for the 3-, 6-, 12-, and 24-atomic cells. The convergence criterion for ions was set to $10^{-4} eV/\text{Å}$.

ZrO_2			no 14	C2h-5	$P2_1/c$	HfO_2			no 14	C2h-5	$P2_1/c$
a,b,c			5.1286	5.2083	5.2962	a,b,c			5.0946	5.1749	5.2687
α, β, γ			90.	99.637	90.	α, β, γ			90.	99.616	90.
Zr	1	4e	0.2772	0.4567	0.7095	Hf	1	4e	0.2772	0.4570	0.7083
O	1	4e	0.0696	0.1643	0.8420	O	1	4e	0.0712	0.1628	0.8410
O	2	4e	0.5512	0.2424	0.5205	O	2	4e	0.5512	0.2424	0.5205

ZrO_2			no 29	C2v-5	$Pca2_1$	HfO_2			no 29	C2v-5	$Pca2_1$
a,b,c			5.255	5.049	5.070	a,b,c			5.226	5.016	5.040
α, β, γ			90.	90.	90.	α, β, γ			90.	90.	90.
Zr	1	4a	0.5312	0.7329	-0.0028	Hf	1	4a	0.5328	0.7325	-0.0028
O	1	4a	0.8670	-0.0698	0.8582	O	1	4a	0.8680	-0.0718	0.8596
O	2	4a	0.7681	0.4620	0.2500	O	2	4a	0.7660	0.4597	0.2489

ZrO_2			no u61	D2h-15	u Pbca	HfO_2			no u61	D2h-15	u Pbca
a,b,c			10.168	5.187	5.295	a,b,c			10.103	5.153	5.270
α, β, γ			90.	90.	90.	α, β, γ			90.	90.	90.
Zr	1	8c	0.3615	0.4575	0.6573	Hf	1	8c	0.3615	0.4579	0.6570
O	1	8c	0.2754	0.7484	-0.0897	O	1	8c	0.2763	0.7475	-0.0894
O	2	8c	0.0323	0.6705	0.8342	O	2	8c	0.0331	0.6692	0.8332

ZrO_2			no a61	D2h-15	a Pbca	HfO_2			no a61	D2h-15	a Pbca
a,b,c			10.043	5.246	5.071	a,b,c			9.976	5.214	5.042
α, β, γ			90.	90.	90.	α, β, γ			90.	90.	90.
Zr	1	8c	0.3847	0.5349	0.2475	Hf	1	8c	0.3847	0.5354	0.2458
O	1	8c	0.2901	0.8750	0.3724	O	1	8c	0.2904	0.8751	0.3721
O	2	8c	0.0225	0.7612	0.5023	O	2	8c	0.0230	0.7615	0.5026

ZrO_2			no 7	Cs-2	Pc	HfO_2			no 7	Cs-2	Pc
a,b,c			10.125	5.242	5.142	a,b,c			10.063	5.209	5.103
α, β, γ			90.	94.603	90.	α, β, γ			90.	94.644	90.
Zr	1	2a	0.3688	0.2139	0.4357	Hf	1	2a	0.3688	0.2132	0.4369
Zr	2	2a	0.1419	0.7108	0.3926	Hf	2	2a	0.1420	0.7103	0.3908
Zr	3	2a	0.8640	0.2121	0.5184	Hf	3	2a	0.8639	0.2115	0.5191
Zr	4	2a	0.6359	0.7145	0.4797	Hf	4	2a	0.6359	0.7136	0.4810
O	1	2a	0.2313	0.0151	0.1609	O	1	2a	0.2306	0.0154	0.1606
O	2	2a	0.2785	0.4949	0.1731	O	2	2a	0.2792	0.4944	0.1725
O	3	2a	-0.0354	0.8963	0.3865	O	3	2a	-0.0355	0.8977	0.3851
O	4	2a	0.5404	0.6218	0.8335	O	4	2a	0.5408	0.6222	0.8334
O	5	2a	0.7276	-0.0067	0.7389	O	5	2a	0.7268	-0.0052	0.7390
O	6	2a	0.7740	0.4907	0.7585	O	6	2a	0.7748	0.4919	0.7586
O	7	2a	0.4645	0.8786	0.3207	O	7	2a	0.4641	0.8782	0.3207
O	8	2a	0.0421	0.6051	0.0205	O	8	2a	0.0421	0.6037	0.0213

ZrO_2			no a62	D2h-16	Pnma	HfO_2			no a62	D2h-16	Pnma
a,b,c			10.300	3.452	3.787	a,b,c			10.203	3.406	3.806
α, β, γ			90.	90.	90.	α, β, γ			90.	90.	90.
Zr	1	4c	0.8809	0.2500	0.2489	Hf	1	4c	0.8817	0.2500	0.2502
O	1	4c	0.7160	0.2500	-0.0979	O	1	4c	0.7152	0.2500	-0.0790
O	2	4c	0.4737	0.2500	0.7402	O	2	4c	0.4741	0.2500	0.7394

ZrO_2			no 31	C2v-7	$Pmn2_1$	HfO_2			no 31	C2v-7	$Pmn2_1$
a,b,c			3.465	5.182	3.752	a,b,c			3.403	5.130	3.787
α, β, γ			90.	90.	90.	α, β, γ			90.	90.	90.
Zr	1	2a	0.0000	0.2603	0.4925	Hf	1	2a	0.0000	0.2627	0.5009
O	1	2a	0.0000	-0.0662	0.8579	O	1	2a	0.0000	-0.0686	0.8399
O	2	2a	0.0000	0.4453	-0.0162	O	2	2a	0.0000	0.4459	-0.0065

ZrO_2			no 137	D4h-15	$P4_2/nmc$	HfO_2			no 137	D4h-15	$P4_2/nmc$
a,b,c			3.585	3.585	5.179	a,b,c			3.566	3.566	5.162
α, β, γ			90.	90.	90.	α, β, γ			90.	90.	90.
Zr	1	2b	0.7500	0.2500	0.2500	Hf	1	2b	0.7500	0.2500	0.2500
O	1	4d	0.2500	0.2500	-0.0483	O	1	4d	0.2500	0.2500	-0.0495

ZrO_2			no 215	Td-1	P-43m	HfO_2			no 215	Td-1	P-43m
a,b,c			5.086	5.086	5.086	a,b,c			5.065	5.065	5.065
α, β, γ			90.	90.	90.	α, β, γ			90.	90.	90.
Zr	1	1b	0.5000	0.5000	0.5000	Hf	1	1a	0.0000	0.0000	0.0000
Zr	2	3d	0.5000	0.0000	0.0000	Hf	2	3c	0.0000	0.5000	0.5000
O	1	4e	0.7756	0.7756	0.7756	O	1	4e	0.2767	0.2767	0.2767
O	2	4e	0.2695	0.2695	0.2695	O	2	4e	0.7702	0.7702	0.7702

ZrO_2			no 225	Oh-5	Fm-3m	HfO_2			no 225	Oh-5	Fm-3m
a,b,c			5.063	5.063	5.063	a,b,c			5.042	5.042	5.042
α, β, γ			90.	90.	90.	α, β, γ			90.	90.	90.
Zr	1	4b	0.5000	0.5000	0.5000	Hf	1	4b	0.5000	0.5000	0.5000
O	1	8c	0.2500	0.2500	0.2500	O	1	8c	0.2500	0.2500	0.2500

2 VIBRATIONAL MODES

For the calculation of the vibrational modes Abinit, see Gonze (2020), and the density functional perturbation theory was used. The structures were relaxed with the local density approximation. The k-point setting and force constraint was chosen as in the structural calculations. The irreducible representations of the vibrational modes is documented in Aroyo et al. (2006). The calculated Raman modes were identified according to the symmetry of the calculated Raman tensor. The calculated infrared modes are classified into TO and LO in Abinit. All the mode frequencies listed below were compared with the Raman and infrared spectra, where TO modes are indicated in the dielectric constant and LO modes in the reflectivity. The pairing of the LO and TO modes is uniquely possible.

2.1 m-phase, monoclinic $\boldsymbol{P2_1/c}$, no 14

The unit cell contains 12 atoms, there are 33 optical phonon modes with the irreducible representation at the zone center

$$9A_g \oplus 9B_g \oplus 8A_u \oplus 7B_u \tag{S1}$$

The A_g and B_g modes are Raman-active, the A_u and B_u modes are IR-active. The results of this work are compared with other simulation Fan et al. (2022) (HfO_2 only) and experimental results for ZrO_2 from Arashi (1992).

14 HfO_2	this work	other simulation: Fan
9 A_g	125, 138, 150, 259, 346, 396, 502, 580, 678	117, 135, 147, 259, 340, 392, 500, 576, 668
9 B_g	136, 170, 247, 336, 410, 520, 560, 643, 782	132, 168, 247, 330, 406, 518, 550, 634, 780
8 A_u(TO)	137, 186, 260, 371, 418, 508, 619, 666	134, 185, 256, 362, 415, 508, 607, 661
8 A_u(LO)	137, 186, 282, 394, 482, 577, 666, 746	134, 186, 276, 390, 481, 572, 661, 749
7 B_u(TO)	247, 257, 330, 348, 408, 524, 751	240, 255, 330, 345, 403, 518, 741
7 B_u(LO)	257, 260, 467, 365, 517, 652, 815	254, 270, 340, 370, 511, 655, 802
	experiment: Arashi	
9 A_g	113, 133, 149, 256, 323, 382, 498, 577, 672	
9 B_g	133, 164, 242, 336, 398, 520, 551, 640, 872	

The mode frequencies in this work were calculated with LDA, the mode frequencies in Fan et al. (2022) were calculated with PBEsol. the comparison shows a good agreement, but in detail a discrepancy in the order of up to $10cm^{-1}$. There is also a discrepancy to the experimental results.

14 ZrO_2	this work
9 Ag	115, 183, 192, 324, 354, 385, 470, 552, 636
9 Bg	177, 226, 320, 333, 391, 490, 540, 611, 751
8 Au(TO)	183, 186, 260, 371, 418, 508, 619, 666
8 Au(LO)	183, 186, 282, 394, 482, 577, 666, 746
7 Bu(TO)	247, 257, 330, 348, 408, 524, 751
7 Bu(LO)	257, 260, 467, 365, 517, 652, 815

2.2 oI*-phase, orthorhombic nonpolar ***Pbca***, no u61

The unit cell contains 24 atoms, there are 69 optical phonon modes. The Raman and IR-modes have not been classified.

2.3 oI-phase, orthorhombic antipolar ***Pbca***, no a61

The unit cell contains 24 atoms, there are 69 optical phonon modes with the irreducible representation at the zone center

$$9A_g \oplus 9B_{1g} \oplus 9B_{2g} \oplus 9B_{3g} \oplus 9A_u \oplus 8B_{1u} \oplus 8B_{2u} \oplus 8B_{3u} \oplus \tag{S2}$$

The A_g, B_{1g}, B_{2g} and B_{3g} modes are Raman-active, the A_u modes are silent. The B_{1u}, B_{2u} and B_{3u} modes are IR-active. The results of this work are compared with other simulation Fan et al. (2022) (HfO_2 only).

a61 HfO_2	this work	other simulation: Fan
9 A_g	115, 141, 202, 263, 333, 381, 438, 579, 633	113, 139, 200, 260, 334, 380, 438, 575, 626
9 B_{1g}	145, 172, 199, 316, 340, 465, 508, 591, 795	143, 173, 198, 312, 341, 465, 505, 585, 793
9 B_{2g}	115, 135, 251, 259, 347, 502, 581, 629, 713	113, 133, 252, 259, 349, 501, 577, 622, 710
9 B_{3g}	131, 162, 220, 314, 442, 473, 589, 670, 702	130, 161, 220, 310, 442, 470, 585, 663, 701
9 A_u(s)	93, 138, 153, 316, 386, 434, 524, 594, 740	92, 138, 152, 311, 386, 434, 521, 586, 740
8 B_{1u}(TO)	131, 191, 278, 389, 421, 487, 628, 702	129, 190, 276, 390, 421, 485, 622, 698
8 B_{1u}(LO)	191, 315, 316, 414, 479, 602, 686, 730	190, 311, 313, 415, 477, 600, 683, 730
8 B_{2u}(TO)	83, 247, 263, 352, 384, 409, 536, 743	82, 248, 261, 354, 385, 408, 532, 739
8 B_{2u}(LO)	84, 247, 320, 352, 409, 506, 641, 794	83, 249, 317, 355, 408, 502, 643, 793
8 B_{3u}(TO)	188, 202, 223, 353, 365, 421, 581, 656	187, 201, 223, 355, 365, 420, 578, 654
8 B_{3u}(LO)	193, 207, 234, 354, 413, 558, 654, 671	193, 207, 232, 356, 413, 556, 653, 671

a61 ZrO_2	this work
9 A_g	137, 184, 205, 316, 344, 361, 414, 550, 600
9 B_{1g}	173, 214, 286, 308, 420, 444, 563, 638, 677
9 B_{2g}	191, 224, 261, 308, 329, 443, 481, 564, 789
9 B_{3g}	148, 173, 262, 320, 347, 476, 550, 601, 686
9 A_u(s)	118, 172, 202, 310, 378, 420, 494, 563, 717
8 B_{1u}(TO)	173, 251, 274, 382, 411, 458, 594, 678
8 B_{1u}(LO)	172, 254, 301, 397, 454, 578, 667, 735
8 B_{2u}(TO)	102, 256, 310, 346, 384, 413, 506, 716
8 B_{2u}(LO)	104, 290, 324, 362, 412, 476, 640, 789
8 B_{3u}(TO)	181, 250, 281, 339, 361, 408, 548, 651
8 B_{3u}(LO)	203, 250, 282, 343, 395, 532, 651, 682

2.4 mIII-phase, monoclinic polar ***Pc***, no 7

The unit cell contains 24 atoms, there are 69 optical phonon modes. The Raman and IR-modes have not been classified.

2.5 Orthorhombic oIII polar $\boldsymbol{Pca2_1}$ no 29

The unit cell contains 24 atoms, there are 69 optical phonon modes with the irreducible representation at the zone center

$$8A_1 \oplus 9A_2 \oplus 8B_1 \oplus 8B_2 \tag{S3}$$

All optical modes are Raman-active. The A_1, B_1 and B_2 modes are IR-active. The results of this work are compared with other simulation Fan et al. (2022) (HfO_2 only) and experimental results for ZrO_2 from Materano et al. (2022).

29 HfO_2	this work	other simulation: Fan
8 A_1(TO)	127, 167, 261, 340, 353, 398, 476, 616	126, 167, 261, 340, 354, 396, 471, 607
8 A_1(LO)	131, 190, 264, 340, 397, 441, 602, 679	129, 189, 264, 340, 395, 439, 595, 677
9 A_2	131, 145, 156, 313, 420, 496, 597, 673, 697	129, 143, 155, 309, 417, 492, 589, 664, 696
8 B_1(TO)	133, 244, 278, 346, 399, 500, 652, 707	130, 244, 276, 345, 397, 497, 643, 702
8 B_1(LO)	132, 244, 316, 349, 495, 618, 696, 726	131, 310, 349, 349, 492, 615, 690, 724
8 B_2(TO)	147, 246, 251, 344, 407, 536, 568, 751	144, 244, 252, 342, 403, 532, 562, 747
8 B_2(LO)	148, 250, 309, 346, 515, 565, 652, 800	146, 251, 306, 345, 511, 560, 651, 797

29 ZrO_2	this work	experiment: Materano
8 A_1(TO)	129, 190, 308, 340, 366, 380, 458, 579	320, 340
8 A_1(LO)	149, 199, 308, 365, 377, 411, 572, 693	
9 A_2	174, 192, 198, 306, 399, 473, 569, 641, 672	197
8 B_1(TO)	175, 261, 308, 349, 401, 471, 620, 683	620
8 B_1(LO)	175, 286, 310, 365, 467, 599, 675, 727	
8 B_2(TO)	191, 241, 318, 343, 403, 508, 545, 726	550
8 B_2(LO)	196, 279, 329, 353, 488, 545, 650, 795	

The frequency dependent dielectric constant depends on the high-frequency dielectric constant ϵ^∞ (frequency larger than mode frequencies but smaller than bandgap), the mode frequencies and the oscillator strength. The table compares our used values from LDA with the values for PBEsol. The difference from both methods is small that the effect on the dielectric and optical functions in this low energy limit is negligible. The static dielectric constant $\epsilon^0 = \lim_{\omega\to 0}\epsilon(\omega)$ is shown for convenience.

ZrO_2	ϵ^∞_{xx}	ϵ^∞_{yy}	ϵ^∞_{zz}	ϵ^0_{xx}	ϵ^0_{yy}	ϵ^0_{zz}
LDA	5.645	5.354	5.343	26.36	20.95	25.16
PBEsol	5.707	5.392	5.403	28.80	22.49	27.14
HfO_2	ϵ^∞_{xx}	ϵ^∞_{yy}	ϵ^∞_{zz}	ϵ^0_{xx}	ϵ^0_{yy}	ϵ^0_{zz}
LDA	5.148	4.923	4.918	22.23	18.25	20.62
PBEsol	5.268	5.022	5.021	24.59	19.76	22.07

2.6 oIV-phase, orthorhombic $\boldsymbol{Pmn2_1}$, no 31

The unit cell contains 6 atoms, there are 15 optical phonon modes with the irreducible representation at the zone center

$$5A_1 \oplus 3A_2 \oplus 2B_1 \oplus 5B_2 \tag{S4}$$

All modes are Raman-active, the A_1, B_1 and B_2 modes are IR-active.

31 HfO_2	this work
5 A_1(TO)	178, 259, 370, 456, 611
5 A_1(LO)	209, 279, 376, 590, 721
3 A_2	123, 469, 604
2 B_1(TO)	264, 458
2 B_1(LO)	354, 690
5 B_2(TO)	158, 305, 495, 662, 710
5 B_2(LO)	158, 430, 635, 662, 749

31 ZrO_2	this work
5 A_1(TO)	131, 334, 338, 460, 587
5 A_1(LO)	183, 335, 361, 572, 741
3 A_2	156, 443, 597
2 B_1(TO)	237, 445
2 B_1(LO)	314, 724
5 B_2(TO)	195, 304, 471, 643, 674
5 B_2(LO)	195, 409, 628, 649, 724

2.7 oV-phase, orthorhombic antipolar ***Pnma***, no 62

The unit cell contains 12 atoms, there are 33 optical phonon modes with the irreducible representation at the zone center

$$6A_g \oplus 3A_u \oplus 3B_{1g} \oplus 5B_{1u} \oplus 6B_{2g} \oplus 2B_{2u} \oplus 3B_{3g} \oplus 5B_{3u} \tag{S5}$$

The A_2, B_{1g}, B_{2g} and B_{3g} modes are Raman-active, the B_{1u}, B_{2u} and B_{3u} modes are IR-active.

a62 ZrO_2	this work
6 A_g	117, 190, 337, 344, 575, 642
3 B_{1g}	161, 459, 578
6 B_{2g}	206, 242, 379, 463, 635, 740
3 B_{3g}	108, 421, 469
3 A_u(s)	123, 264, 577
5 B_{1u}(TO)	123, 300, 435, 487, 683
5 B_{1u}(LO)	123, 408, 444, 640, 737
2 B_{2u}(TO)	262, 433
2 B_{2u}(LO)	335, 712
5 B_{3u}(TO)	159, 241, 438, 526, 643
5 B_{3u}(LO)	193, 254, 517, 639, 735

a62 HfO_2	this work
6 A_g	110, 188, 261, 367, 603, 666
3 B_{1g}	126, 484, 595
6 B_{2g}	161, 186, 390, 488, 658, 757
3 B_{3g}	88, 440, 493
3 A_u(s)	96, 280, 595
5 B_{1u}(TO)	103, 300, 443, 503, 714
5 B_{1u}(LO)	103, 429, 444, 642, 754
2 B_{2u}(TO)	278, 451
2 B_{2u}(LO)	365, 685
5 B_{3u}(TO)	197, 204, 439, 554, 645
5 B_{3u}(LO)	181, 246, 536, 644, 714

2.8 t-phase, tetragonal $\boldsymbol{P4_2/nmc}$, no 137

The unit cell contains 6 atoms, there are 15 optical phonon modes with the irreducible representation at the zone center

$$1A_{1g} \oplus 2B_{1g} \oplus 3E_g \oplus 1A_{2u} \oplus 1B_{2u} \oplus 2E_u \tag{S6}$$

The A_{1g}, B_{1g} and E_g modes are Raman-active, the A_{2u}, and E_u modes are IR-active, the B_{2u} mode is silent. The results of this work are compared with other simulation Fan et al. (2022) (HfO_2 only) and experimental results for HfO_2 from Quintard et al. (2002), and experimental results for ZrO_2 from Fei (1981), Hirata et al. (1994) and Pecharromán et al. (1996).

137 HfO_2	this work	other simulation: Fan	exp.: Quintard	exp.: Quintard
1 A_{1g}	286	276	262	265
2 B_{1g}	238, 616	240, 609	220, 584	240, 590
3 E_g	109, 475, 684	107, 474, 677	115, 479, 660	117, 485, 640
1 B_{2u}(s)	683	682	exp.: Pecharroman	exp.t: Hirata
1 A_{2u}(TO)	326	321	336	320
1 A_{2u}(LO)	630	633	650	
2 E_u(TO)	120, 468	129, 460	164, 339	140, 550
2 E_u(LO)	263, 713	267, 711	232, 734	

137 ZrO_2	this work	exp.: Feinberg	exp.: Hirata
1 A_{1g}	266	266	257
2 B_{1g}	323, 599	326, 616	305, 595
3 E_g	143, 463, 648	155, 474, 645	..., 465, 630
1 B_{2u}(s)	662	exp.: Pecharroman	exp.: Hirata
1 A_{2u}(TO)	334	336	320
1 A_{2u}(LO)	654	650	
2 E_u(TO)	146, 441	164, 339	140, 550
2 E_u(LO)	261, 727	232, 734	

2.9 c-phase, cubic $\boldsymbol{Fm\bar{3}m}$, no 225

The unit cell contains 3 atoms, there are 6 optical phonon modes with the irreducible representation at the zone center

$$1T_{2g} \oplus 1T_{1u} \tag{S7}$$

The T_{2g} mode is Raman-active, the T_{1u} mode is IR-active. The results of this work are compared with other simulation Fan et al. (2022) (HfO_2 only)

225 HfO_2	this work	other simulation: Fan
1 T_{2g}	606	599
1 T_{1u}(TO)	262	266
1 T_{1u}(LO)	640	643

225 ZrO_2	this work
1 T_{2g}	582
1 T_{1u}(TO)	265
1 T_{1u}(LO)	664

2.10 cII-phase, cubic $\boldsymbol{P\bar{4}3m}$, no 215

The unit cell contains 12 atoms, there are 33 optical phonon modes. The phonon dispersion in Antunes et al. (2022) shows the structure to be dynamically unstable. The calculation of the dielectric constant is therefore not possible.

3 INVERSE PCA, CLUSTER, XRD SPECTRA

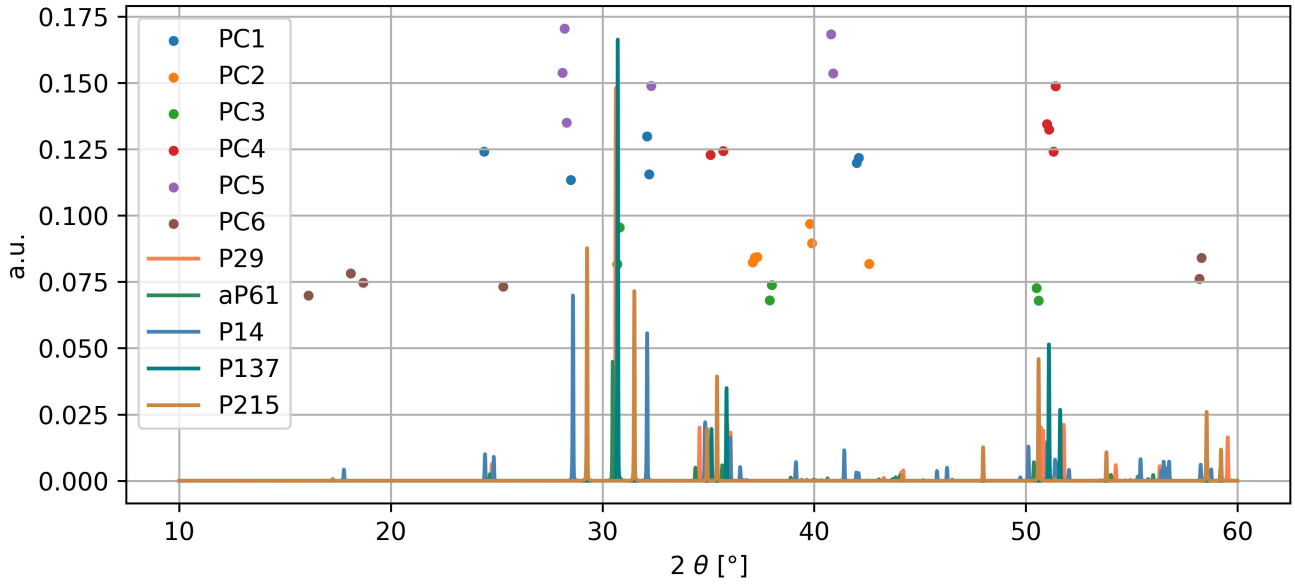

Figure S1. Displayed are the XRD spectra of the undoped phases (lines) and the five largest loadings of the six most influential PCs (dots), visualizing the initial features with the highest data variation.

The inverse PCA reveals the information content of the PCAs. PC1 loosely matches the XRD signature of the m-phase (no 14), which can be understood by strong deviation from the XRDs of the other phases, originating mainly from the monoclinic cell angle. With the other phases sharing their main peak around 30°, and therefore resembling low data variance in this area, the other PC describe secondary, more distinguishable peaks of the different phases.

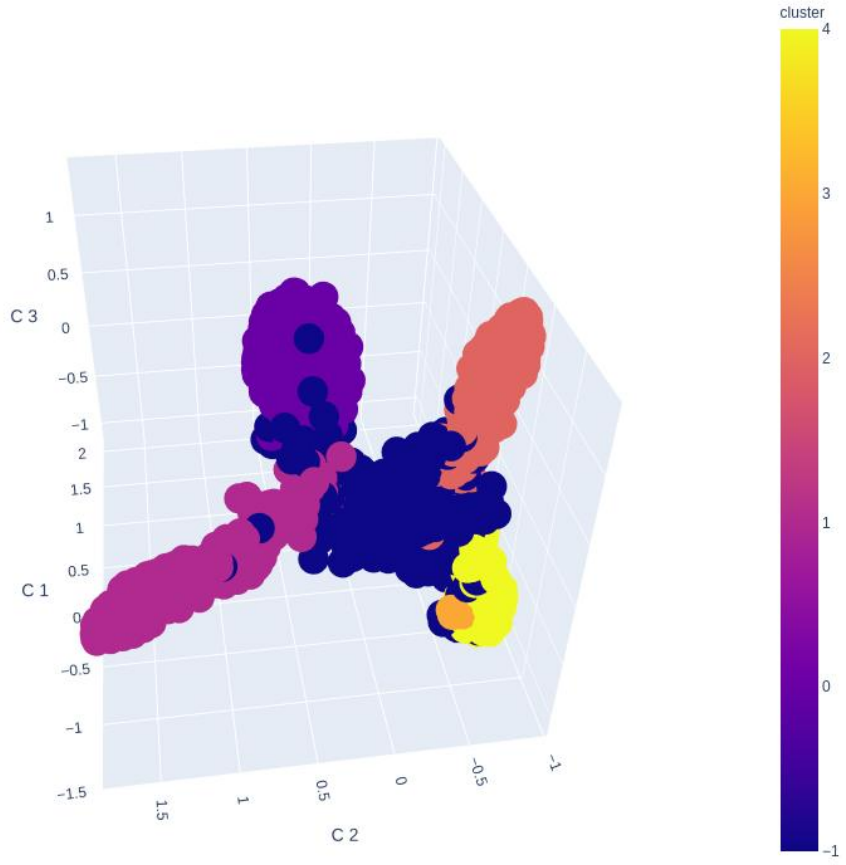

Figure S2. Clustering of the HfO_2 data after feature reduction with PCA to 50 degrees of freedom.

The outlier cluster cannot uniquely be decomposed into further subcluster. But the outlier cluster contains all the phases documented in this work, which have not been prepared as initial structure.

HfO_2 no 31	HfO_2 no 62
HfO_2 no 7	HfO_2 no u61

Figure S3. Displayed are the XRD-spectra of different HfO_2-structures occurring in the data-set. Resulting from the small occurrence in the data-set and the low intensity of the distinctive peaks, results the impossibility of a reliable clustering of the spectra.

REFERENCES

(1981). Structural disorder and phase transitions in zro2-y2o3 system. Journal of Physics and Chemistry of Solids 42, 513–518. doi:https://doi.org/10.1016/0022-3697(81)90032-9

Antunes, L. A., Ganser, R., Kuenneth, C., and Kersch, A. (2022). Characteristics of low energy phases of hafnia and zirconia from dft calculations. physica status solidi (RRL) – Rapid Research Letters 0, 0. doi:https://doi.org/10.1002/pssr.202100636

Arashi, H. (1992). Pressure-induced phase transformation of hfo2. Journal of the American Ceramic Society 75, 844–847. doi:https://doi.org/10.1111/j.1151-2916.1992.tb04149.x

Aroyo, M. I., Perez-Mato, J. M., Capillas, C., Kroumova, E., Ivantchev, S., Madariaga, G., et al. (2006). Bilbao crystallographic server i: Databases and crystallographic computing programs. Zeitschrift für Kristallographie 221, 15–27

Blum, V., Gehrke, R., Hanke, F., Havu, P., Havu, V., Ren, X., et al. (2009). Ab Initio Molecular Simulations with Numeric Atom-Centered Orbitals. Comput. Phys. Commun. 180, 2175–2196. doi:10.1016/j.cpc.2009.06.022

Fan, S., Singh, S., Xu, X., Park, K., Qi, Y., Cheong, S. W., et al. (2022). Vibrational fingerprints of ferroelectric hfo2. npj Quantum Materials 7, 1. doi:https://doi.org/10.1038/s41535-022-00436-8

Gonze, X. (2020). The abinitproject: Impact, environment and recent developments. Computer Physics Communications 248, 107042. doi:https://doi.org/10.1016/j.cpc.2019.107042

Hirata, T., Asari, E., and Kitajima, M. (1994). Infrared and raman spectroscopic studies of zro2 polymorphs doped with y2o3 or ceo2. Journal of Solid State Chemistry 110, 201–207. doi:https://doi.org/10.1006/jssc.1994.1160

Materano, M., Reinig, P., Kersch, A., Popov, M., Deluca, M., Mikolajick, T., et al. (2022). Raman spectroscopy as a key method to distinguish the ferroelectric orthorhombic phase in thin zro2-based films. physica status solidi (RRL) – Rapid Research Letters 16, 2100589. doi:https://doi.org/10.1002/pssr.202100589

Pecharromán, C., Ocaña, M., and Serna, C. J. (1996). Optical constants of tetragonal and cubic zirconias in the infrared. Journal of Applied Physics 80, 3479–3483. doi:10.1063/1.363218

Quintard, P. E., Barbéris, P., Mirgorodsky, A. P., and Merle-Méjean, T. (2002). Comparative lattice-dynamical study of the raman spectra of monoclinic and tetragonal phases of zirconia and hafnia. Journal of the American Ceramic Society 85, 1745–1749. doi:https://doi.org/10.1111/j.1151-2916.2002.tb00346.x